EVALUATION OF SOME RECENT JET NOISE REDUCTION CONCEPTS*

C. Kannepalli[†], D.C. Kenzakowski[††] and Sanford M. Dash[†††]
Combustion Research and Flow Technology, Inc. (CRAFT Tech®)
Dublin, PA 18917
kchandra@craft-tech.com

Abstract

This paper discusses RANS based numerical simulations of a 1/10th scale over-expanded supersonic plume (resembling that of an F-18 aircraft) with chevrons used as "passive" noise reduction devices. Three variant designs of the chevrons mounted in specified azimuthal arrangements around the baseline nozzle exit are evaluated. A major effect of the chevrons is to amplify the Mach disc size and move it closer to the nozzle exit. For these over-expanded exhausts, the chevrons must extend sufficiently deep into the plume core stream to reduce jet noise levels. Results from our simulations are in "nominal" accord with the experimental observations (primarily noise measurements) as ascertained by examining the flow structure, and via using jet noise prediction codes. Evaluation of the thrust loss produced by these devices is found to be minimal except for the one chevron configuration that provided maximum noise reduction. Our studies indicate that noise reduction devices which work for laboratory model jets may have to be revised to have them work for the real engine due to complexities in the internal mixing which cannot be replicated at laboratory scale. We discuss issues related to these differences and with real aircraft effects such as plume/plume interactions and installation effects, and we present a complete aircraft/dual engine plume simulation using innovative multi-element unstructured gridding.

1.0 Introduction

While substantial work has been performed over the years to minimize the IR signature of military jet exhausts, only recently has attention been focused on the jet noise [1]. Laboratory experiments being performed by Seiner at U.Miss. and Krothapalli at FSU are investigating a variety of passive (non-pulsatile) jet noise reduction concepts that include use of chevrons, micro-jets, and hybrid concepts. CRAFT Tech® has been using RANS CFD methodology to evaluate and refine these varied concepts. Our CFD simulations have been in "nominal" accord with the experimental observations (primarily noise measurements) as ascertained by examining the effect a concept has on the jet turbulence and shock structure, and via using simplistic noise correlations as well as noise prediction codes that are in a preliminary state of development. We also have evaluated thrust modification produced by these devices.

Of most significance in the use of RANS CFD is its ability to identify how a passive noise reduction concept modifies the flow structure. CFD clearly shows that for a chevron to be effective, its sizing and placement is quite critical. The jet flows studies discussed here relate to the jet exhaust of an F/A 18 E/F aircraft. At flight conditions of interest (where jets on training missions produce excessive noise in civilian areas – see Ref [2]), jet exhaust is over expanded and has a multiple-cell shock structure with Mach discs. The nozzle contains a plug and thus the initial centerline region of the jet has a mass defect from the plug wake. Laboratory models have simulated the basic geometry but cannot simulate the extremely complex internal mixing [3]. As such, the laboratory model jet exhausts are fully mixed internally while the real engine exhaust is only partially mixed. Our studies indicate that noise reduction devices which work for the laboratory model jets may have to be revised considerably to have them work for the real engine, which is a major role provided by CFD.

Also of concern for this aircraft is the role played by plume/plume interactions and by installation effects. The nozzle axes are inclined towards each other and the engines are closely spaced. Simulating these effects, and predicting how well the noise reduction concepts perform under varied flight conditions is a critical role being performed by CFD.

In this paper, we will first briefly describe the RANS CFD methodology utilized which emphasizes the need to highly resolve the flow in the immediate vicinity of the noise reduction device. This entails use of a parallel architecture framework with domain-decomposition, supplemented by the use of non-contiguous interfacing with flux preservation. We next review laboratory chevron studies whose arrangement is shown in Figure 1.

*AIAA-2003-3313, 9th CEAS/AIAA, Meeting, Hilton Head, SC, May 12-14, 2003.
[†] Research Scientist, Member AIAA
[††] Senior Research Scientist, Member AIAA
[†††] President & Chief Scientist, Associate Fellow AIAA

Report Documentation Page

Form Approved
OMB No. 0704-0188

1. REPORT DATE	2. REPORT TYPE	3. DATES COVERED
2003		**00-00-2003 to 00-00-2003**

4. TITLE AND SUBTITLE	5a. CONTRACT NUMBER
Evaluation of Some Recent Jet Noise Reduction Concepts	5b. GRANT NUMBER
	5c. PROGRAM ELEMENT NUMBER
6. AUTHOR(S)	5d. PROJECT NUMBER
	5e. TASK NUMBER
	5f. WORK UNIT NUMBER
7. PERFORMING ORGANIZATION NAME(S) AND ADDRESS(ES) **Combustion Research and Flow Technology Inc (CRAFT Tech),6210 Keller's Church Road,Pipersville,PA,18947**	8. PERFORMING ORGANIZATION REPORT NUMBER
9. SPONSORING/MONITORING AGENCY NAME(S) AND ADDRESS(ES)	10. SPONSOR/MONITOR'S ACRONYM(S)
	11. SPONSOR/MONITOR'S REPORT NUMBER(S)

12. DISTRIBUTION/AVAILABILITY STATEMENT
Approved for public release; distribution unlimited

13. SUPPLEMENTARY NOTES
The original document contains color images.

14. ABSTRACT

15. SUBJECT TERMS

16. SECURITY CLASSIFICATION OF:			17. LIMITATION OF ABSTRACT	18. NUMBER OF PAGES	19a. NAME OF RESPONSIBLE PERSON
a. REPORT	b. ABSTRACT	c. THIS PAGE			
unclassified	**unclassified**	**unclassified**		**17**	

Standard Form 298 (Rev. 8-98)
Prescribed by ANSI Std Z39-18

Lastly, we touch upon issues associated with differences between laboratory models and real engines, and with plume/plume and installation effects.

2.0 Overview of CFD Methodology and Simulation parameters

All simulations were performed using the CRAFT CFD structured grid Navier-Stokes code. The CRAFT CFD code is a finite-volume, fully implicit, Roe/TVD solver that has been used extensively for jet simulations studying noise reduction concepts and aircraft plume IR signatures [4-7]. A number of capabilities exist in CRAFT that make it suitable for advanced jet simulation studies, and these are highlighted below. For all simulations described, a perfect gas equation of state (γ=1.4) and a constant turbulent Prandtl number of 0.9 were assumed, and a corrected k-ε turbulence model that is well calibrated for high-speed supersonic flows was used [8]. Table 1 summarizes the principal features of this model.

Table 1. Aeropropulsive kε-Model.
• Baseline high Re jet coefficients (Launder – 1972) • Unified compressibility correction (cc) and compressible vortex stretching correction • Modified So-Zhang (sz) low Re and compressible wall function near wall models
DEVELOPMENTAL
• Weak shear correction • Scalar Fluctuation Equations (k_T/ε_T, $k_\alpha/\varepsilon_\alpha$) • Variable Pr_t/Sc_t Model • Curvature/High Strain/Swirl Corrections

The grid blanking methodology in the CRAFT CFD® code increases its versatility for flowfield problems involving complex geometries. This feature works in conjunction with the implicit ADI procedure for inverting the matrix arrays in the direction of the implicit sweep. Grid blanking also facilitates structured mesh generation by allowing the grids to better conform to the specified geometry and flow direction and minimize "skewness." User-specified boundary conditions along internal and external grid surfaces allow for automatic construction of patches, or sweeps, in each computational direction. Moreover, wall boundaries do not need to coincide with inter-block boundaries. This allows for a more generalized placement of interior boundary conditions away from regions that are likely to interfere with shear layer development and restrict time advancement.

The boundary layer region is an important aspect of the nozzle flowfield. It is therefore important to accurately predict the mass deficit effect of the boundary layer to assess nozzle performance. In addition, boundary layer turbulence can impact the downstream plume shear layer development, especially for the core/fan mixing region where velocity ratios are small. Resolution of the boundary layer flowfield near the wall would require tightly packed grids of high cell aspect ratio, which increases storage and CPU costs (more grid points needed) and often hinders solution convergence due to the small local time steps required. In an effort to reduce the costs for resolving viscous wall effects, a compressible law of the wall model [9] has been implemented in CRAFT and was used for both the axisymmetric and 3D simulations. Wall functions analytically relate surface boundary conditions to points in the inertial sublayer region, where the shear stress is assumed constant. In this study, the grid resolution employed ensured that the first cell location off the wall was less than a y+ of 25 and a minimum of eight grid points were below a y+ of 300. This latter constraint was made to provide a reasonable estimate of momentum deficit effects on the flowfield exhaust (e.g. mass flow rates). For the present studies, adiabatic walls were assumed.

The solution of the 3D nozzle exhaust flowfields required around one million grid cells. To boost solution turnaround time, a domain decomposition strategy was employed for distributing the overall computational volume across a user-specified number of processors and running the CRAFT CFD® code in parallel via the Message Passing Interface (MPI) library. This domain decomposition procedure allows for linear solution speedup on parallel architectures and operates independently of the patching methodology described above. This feature enables the user to focus grid construction based on flowfield resolution requirements and not on processor load balancing. This also allows for placement of potential inter-block boundary interference away from regions of shear layer evolution.

Another feature of the CRAFT CFD® code is the use of non-contiguous boundaries. At these boundaries (preferably located in "quiet" regions of the flow) grids can be discontinuous and help reduce the number of grid points used in the simulation. Figure 2(b) illustrates a non-contiguous grid at the axis in the simulation where 41 grid points from above is reduced to 11 grid points in the azimuthal direction towards the axis. The use of such boundaries close to the axis in 3D simulations also helps in convergence as the number of points converging on the axis is reduced. Simulations have

been performed with and without these boundaries at the axis and the solutions verified so that these boundaries do not effect the solution.

Subsonic conditions were imposed at the nozzle inflow boundary using the specified total pressure and total temperature and these correspond to a nozzle NPR = 3.94 and To = 1020 K. These conditions correspond to the laboratory nozzle with fully mixed internal flow and closely corresponds to the aircraft with engines at take-off thrust setting but standing still on the runway. The plug in the nozzle was also simulated to account for the wake-like profiles that would be present due to the same at the nozzle exit. Three different chevron geometries were tried out with 6 or 12 chevrons arranged azimuthally in 60 or 30 degree sectors around the nozzle (see Figure 1). For the 12 chevron configuration the percentage of projected area of chevron to the nozzle exit area for chevron 1 is 2.2%, for chevron 2 is 3.5% and for chevron 3 is 12% respectively. Chevron 1 is inclined along the nozzle cowling at an angle of ~20 deg. from the horizontal and canted into the core while chevron 2 and chevron 3 are canted at ~ 38 deg. Chevron 1 and chevron 2 were run in both 6 and 12 configurations while chevron 3 was run only in a 12 configuration arrangement.

A $1/10^{th}$ scale nozzle with exit diameter of 2.06" was used for all the simulations. The streamwise length of the computational domain extended 20 nozzle exit diameters downstream of the nozzle exit and included the entire jet growth in the radial direction. Based on the geometric configurations of 6 or 12 chevrons used, fifteen or thirty-degree symmetry was assumed for the 3D flowfields. Both the baseline and 3D chevron grids were constructed with similar wall mesh density to minimize boundary layer resolution effects in the subsequent flowfield comparisons. Grids were packed radially along all wall surfaces and axially near the nozzle exits and chevrons. The baseline grid is also 3D and was selected to facilitate flowfield comparisons and to provide a good initial flowfield solution for the 3D cases. Figure 2 illustrates the grid distribution around the nozzle exit and the chevron; the purple colored chevron is chevron 1, orange colored chevron is chevron 2 and red colored chevron is chevron 3 extension of chevron 2. The total grid points for these calculations ranged from 1 to 1.5 million.

2.1 Corrected k-ε turbulence model validation

Figure. 3 shows a validation study of the corrected k-ε model as applied to M = 2.0 hot jet of Seiner et al. [10]. Figures 3(a) and (b) show the comparison of the centerline streamwise velocity and temperature respectively for the jet compared with the experiment. One can see that the standard k-ε model predicts a faster decay of the jet core velocity while the corrected k-ε model captures the correct decay. The slower decay is primarily due to the compressibility corrections (CC) decreasing the turbulence levels when compared to the standard model. Compressible vortex-stretching (CVS) corrections have only a small affect for high speed jets.

2.2 Effect of internal plug in nozzle

Figure 4.1 shows the contours of Mach number, pressure, temperature and turbulent kinetic energy (TKE) in the xy plane for the baseline nozzle that illustrates the effect of the internal plug. The presence of this plug acts like a blunt body and leads to wake-like distributions of the various nozzle exit physical quantity profiles, the most significant from turbulence perspective being a non-zero TKE along the jet axis. This effect needs to be correctly captured as results downstream of the nozzle exit will be very much influenced by it.

2.3 Effect of turbulence model

Figure 4.2(a) shows the contours of TKE in the xy plane for the baseline nozzle with the standard k-ε (upper half) and the corrected k-ε model (lower half). One can see that the TKE is decreased due to compressibility corrections present in the corrected model and also the shear layer that develops from the lip of the nozzle exit is thinner than that with the standard model. The axial variation of TKE and stagnation temperature shown in Figures 4.2(b) and (c) respectively, reveal the differences caused by the corrected model that include a decrease in the TKE/turbulence levels and a lengthening of the jet core. The stagnation temperature variation shows that the mixing is reduced by compressibility as also from a lengthening of the jet core. ***All results shown henceforth will involve simulations performed with this corrected k-ε model that is physically a better model for such high-speed flows.*** The jet in the present study has nominal exit M=1.6 and in the earlier section this model has been validated for a hot jet of M=2.0.

3.0 Chevron Laboratory Studies

This section discusses the results of the nozzle fitted with the three chevron designs (in both in 6 and 12 azimuthal configuration) and compares them with those of the baseline nozzle.

From a RANS CFD perspective some insight into jet noise can be obtained from the jet centerline distribution of the static pressure and turbulent kinetic energy. Figure 5 shows the jet

centerline distribution of Mach number, static pressure and TKE for all the nozzle configurations studied. For chevron 1 and chevron 2 in both configurations of 6 or 12 chevrons around the nozzle exit, there are small differences in the solution. Differences in the number of chevrons had a minimal effect on the flow structure and, most results that will be presented will be restricted to the 12 chevron configuration unless specifically mentioned.

Chevron 3 causes the most appreciable change to the flow structure. Pressure excursions in the shock cells are not attenuated but the entire shock cell pattern is shifted upstream closer to the nozzle exit. Based on a crude turbulence-to-noise argument, if the peak TKE levels at a given downstream location from the nozzle exit (typically in the noise producing region, in the vicinity of where the jet core ends) are lowered by the use of chevrons, then one can argue that the noise production by this turbulence would be lower. Figure 6(a) shows the axial distribution of the peak TKE values while 6(b) shows the integrated TKE distribution that was generated using the following formula:

$$\frac{\int kdm}{\int dm},$$

where *dm* is the mass flow rate at any streamwise section with exception made for the mass flow rate in the free stream. The peak TKE levels decrease in the near vicinity of the chevron for all cases but only for Chevron 3 is the effect global (i.e., the integrated TKE levels are lower than the baseline levels) and thus chevron 3 is providing the most substantive effect at reducing turbulence.

Figures 7, 8 and 9 show the contours of TKE and Mach number for chevrons 1, 2 and 3 respectively, compared with the baseline nozzle and the corresponding velocity vectors in the near vicinity of the chevron. Note the velocity vectors (colored by the streamwise u-velocity) are plotted with equal magnitude to highlight the re-circulation region. As seen earlier with the axial distributions, chevrons 1 and 2 do not produce appreciable changes to the flow. The small change they produce is to amplify the Mach disc and move it closer to the nozzle exit. Chevron 3 does the same but the effect is a lot stronger and more significant. A stronger Mach disc can be seen closer to the nozzle exit and the turbulence is greatly amplified accompanied by a reduction in the jet core.

A comparison of the velocity vectors in the near vicinity of the chevrons for the three cases reveals that chevron 1 and chevron 2 disturb the boundary layer from the nozzle walls to a small extent while chevron 3 causes a large re-circulation region that penetrates past the boundary layer and into the core of the jet. In the symmetry plane between chevrons, chevron 3 configuration shows some v and w-velocity vectors contours (Figure 10) that cause some local mixing of the flow. This explains why chevron 3 is so effective in disturbing the flow structure. Figure 10 shows the TKE, Mach number and v/w velocity contours in the cross-stream plane (in 90 deg sectors) for all the 3 chevrons in the 12 chevron configuration compared to the baseline nozzle. One can see although the effect of the chevron is locally limited ($x/R < 5$), it is sufficient to disturb the flow and turbulence structure. It can hence be seen that the location, angle and depth to which a chevron extends into the jet core is quite critical in how effective it can be in altering the flow structure and subsequently account for noise suppression. Chevrons 1 and 2 are not effective, a finding that has been corroborated by experimental findings.

3.1 Noise predictions

Studying such noise reduction concepts by RANS can reveal the change that these concepts are producing to the flow and turbulence structure and thus how effective they are in reducing noise on a relative basis. Relating these changes towards their qualitative effect on noise suppression is still an active area of research. Preliminary evaluations (using NASA jet noise research code Jet3D [11]) of the RANS solutions obtained is currently in progress and Figure 11 shows the OASPL prediction (for observers on an arc of radius equivalent to 55 jet exit diameters from the nozzle exit) by Jet3D for the baseline nozzle compared with that of Seiner's experiment. An observer angle of zero corresponds to a location on the jet centerline downstream of the nozzle exit and an angle of 180 corresponds to the same upstream of the nozzle exit. There is good agreement with the experimental data for observer angles in the range 50-150 degrees. One can see that the effect of turbulence model is also seen in the noise predictions in that the corrected k-ε model captures the physics of high-speed jets better and hence the noise level predictions are also closer to that of the experiment. Further tests and evaluation of using NASA jet noise codes is underway for gaining confidence in obtaining reliable "relative" noise level predictions.

3.2 Thrust Implications

The use of chevrons at the exit of the nozzle is believed to help reduce noise but it comes with a penalty of loss in thrust. Evaluating this penalty is

critical in the design of the "optimal" chevron configuration that gives maximum noise reduction with minimal loss in thrust. For the laboratory nozzle/chevron configurations considered in the study above, a thrust prediction calculation was performed. The methodology used assumes a control volume that includes the inlet, the internal wetted-walls of the nozzle inclusive of the chevron and the exit of the nozzle at the end of the chevron as shown in Figure 12. The total momentum in the axial direction coming into the nozzle is the same for all configurations and when the axial force of the walls on the nozzle flow (which is different for the different chevrons) is subtracted, we get the net momentum exiting the nozzle. This simple and "ideal" control volume method of determining the thrust, however, assumes that the total mass in the assumed control volume is conserved but in the present case is not "exactly" true. There is a small amount of mass that is entrained at the nozzle exit, which is difficult to account for, and hence neglected. However since this mass is a very small fraction of the incoming nozzle mass flow, it is quite acceptable to neglect it and thus the thrust prediction is reasonable to this extent. Table 2 shows the thrust calculation for the various chevron configurations. One can see that chevron 3 has the worst thrust penalty of 5.7% while chevron 1 and 2 both are within 1.2%.

All simulations thus far have involved laboratory conditions. How the real flow nozzle may further effect the performance of these devices will be discussed in the next section.

4.0 Real Aircraft/Engine Considerations

Downstream of the turbine exit station, the internal core/bypass mixing within an actual nozzle consists of a complex series of discrete slot jets and other mixing passages [1]. In contrast, current laboratory simulations assume a single (fully mixed) stream and a simplified augmentor flow path. The impact of this assumption on downstream plume mixing is significant and is illustrated in the following comparative numerical simulations. Two nozzle/plume simulations at the same engine cycle conditions were considered: one representative of the real engine bypass mixing along the engine augmentor and one representing the uniform mixing assumptions of laboratory experiments but at full engine scale. Figure 13 compares the resulting Mach number contours of the two simulations and indicates that the "realistic" nozzle yields a shorter jet core length. A significant factor in this result is the large levels of turbulence upstream of the nozzle exit produced by the series of slot jet mixing layers, as shown in Figure 14. Additionally, the temperature comparisons of Figure 15 show that the exhaust of the "realistic" nozzle is highly non-uniform, with partially mixed bypass flow along the outer nozzle region. Figure 16 shows the radial exit plane distribution of velocity, static temperature and TKE for the realistic nozzle configuration and for the laboratory equivalent nozzle. For the real nozzle one can see the effect of internal bleed/mixing to create a larger boundary layer for both temperature and velocity with accompanying higher levels of TKE and lower wall temperatures. It seems that a chevron designed for the laboratory nozzle may be ineffective for the real configuration because of the differing boundary layers present. In this regard, CFD can help illuminate such real flow effects easily and further help in picking the ideal location, size and optimal design for maximum effectiveness of these devices in providing the noise suppression levels desired.

Another area studied was that of plume/plume interactions. On the real aircraft, the nozzles are canted inwards at about 2° towards the vehicle centerline. As shown in Figure 17, for military thrust (MRT) conditions in a static surrounding flow, the plumes coalesce quite early (well before the end of the potential core on each jet). Hence, peak noise will be strongly affected by these interactions. In contrast, for a higher altitude situation at cruise rate thrust (CRT) with a transonic flight velocity, the plumes do not coalesce as quickly as shown by the TKE contours of Figure 18.

The last area examined is that of interactions with the vehicle aerodynamics. Figure 19 shows the very detailed multi-element unstructured grid required to resolve the plume structure properly. Figures 20 show some details of the plume structure while Figure 21 compares the structure of a single isolated plume, of dual plumes without aerodynamic effects, and of dual plumes with the complete aerodynamic solution.

5.0 Conclusions

This paper has presented preliminary work towards investigating chevrons as noise reduction concepts of relevance to military fighter aircraft. For conditions of interest the exhaust is overexpanded, there is an internal plug, and the plume has a complex shock structure including Mach discs. We had first analyzed a laboratory model of this aircraft nozzle that mimics the real geometry but does not represent the complex core/fan mixing occurring internally. We found that since the exhaust was over-expanded, the actuation provided by the noise reduction devices would have to be larger than those for perfectly or under expanded plumes, since the plume turns inward (contracts) at the nozzle lip and the device must

penetrate to the high speed core to be effective. Figure 22. Comparisons of the plume of laboratory and real engines (generic) look somewhat comparable, but the exit plane profiles differ with the real nozzle exit plane having a much larger low velocity region. This implies that we cannot simply scale-up from lab studies but must use CFD with a real engine exhaust to design these devices. .

Work now in progress includes:

- Sizing of the concepts to achieve effective noise reduction on a real engine.
- Use of new hybrid concepts
- Use of droplet/polymer injection; and,
- Examination of plume/plume interaction and full aerodynamic/installation effects under varied conditions
- Use of noise prediction codes with CFD to help evaluate noise effectiveness of various designs.

6.0 Acknowledgements

Portions of this work were funded by ONR/Dr. Gabriel Roy. The authors also thank Dr. Craig Hunter for discussions and the use of the noise code Jet3D.

7.0 References

[1] Dash, S.M., Kenzakowski, D.C. Kannepalli, C., Chenoweth, J.D. and Sinha, N., "CFD Simulations Of Supersonic Jet Noise Reduction Concepts," Proceedings of the Fifteenth ONR Propulsion Meeting, Washington, DC, pp. 136-142, August 5 to 7, 2002.

[2] Seiner, J.M., Jansen, B.J., Ukeiley, L, Ponton, M.K., " Acoustic Fly-Over Studies of F/A-18 E/F Aircraft During FCLP Mission," ONR BAA 01-016, Jet Noise Suppression Technologies for Military Aircraft, Task 1: Final Report, NCPA, U. MISS, December 2002.

[3] Cavallo, P.A., Kenzakowski, D.C., and Dash, S.M., "Axisymmetric Flowfield Analysis of the F414-400 Turbofan and Exhaust Plumes," Final Report, Combustion Research and Flow Technology, Inc., Report No. CRAFTR-10/97.014, October 1997.

[4] Dash, S.M., Kenzakowski, D.C., Perrell, E.R., Cavallo, P.A., Chidambaram, N., and Sinha, N., "Advances in Simulation of Passive Jet Noise Reduction," AIAA-98-2268 4th AIAA/CEAS Joint Aeroacoustics Conference, Toulouse, France, June 2–4, 1998.

[5] Kenzakowski, D.C., and Dash, S.M., " Study Of Three-Stream Laboratory Jets With Passive Mixing Enhancements For Noise Reduction," AIAA Paper No. 2000-0219, 38th AIAA Aerospace Sciences Meeting at Reno, NV, Jan 10-13, 2000.

[6] Kenzakowski, D.C., Shipman, J. and Dash, S.M., "Towards Simulating Non-Axisymmetric Influences on Aircraft Plumes for Signature Prediction," 2000 JANNAF EPTS & SPIRITS User Group Joint Meeting, Nellis Air Force Base, Las Vegas, NV, May 15-19, 2000.

[7] Kenzakowski, D.C., Shipman, J.D., Dash, S.M., Markarian, P. Borger, M. and Smith, G., "Increasing Fidelity Of Aircraft Plume IR Signatures," The 2001 Electromagnetic Code Consortium (EMCC) Annual Meeting, Kauai, Hawaii, 28 May-1 June 2001.

[8] Papp, J.L. & Dash, S.M., "Turbulence model unification and assessment for high-speed aero-propulsive flows", AIAA-2001-0880, *39th AIAA, Aerospace Sciences Meeting and Exhibit*, Reno, NV, Jan 2001.

[9] Kenzakowski, D.C., and York, B.J., "Inclusion of Compressible Wall Function Methodology Into CRAFT Navier-Stokes Code; Task 3, part 2: Wall Function," CRAFTR-2/97.003.

[10] Seiner, J.M., Ponton, M.K., Jansen, B., and Lagen, N.T., "The effects of Temperature on Supersonic Jet Noise Emission," DGLR/AIAA 14th Aeroacoustics Conference, Aachen GE, May 1992.

[11] Hunter, C.A., and Thomas, R.H., "Development of a Jet Noise Prediction Method for Installed Jet Configurations," 9th AIAA/CEAS Conference and exhibit, 12-14 May 2003/ Hilton Head, SC.

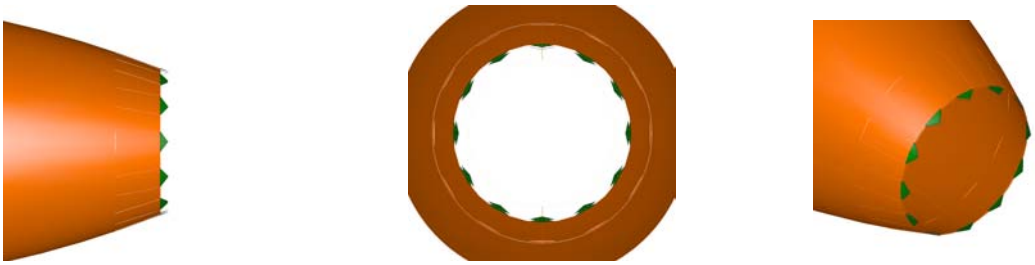

Figure 1. Arrangement of Chevrons (green in color and 12 in number) at the Nozzle Exit. For the 6 Configuration Every Other Chevron is Removed.

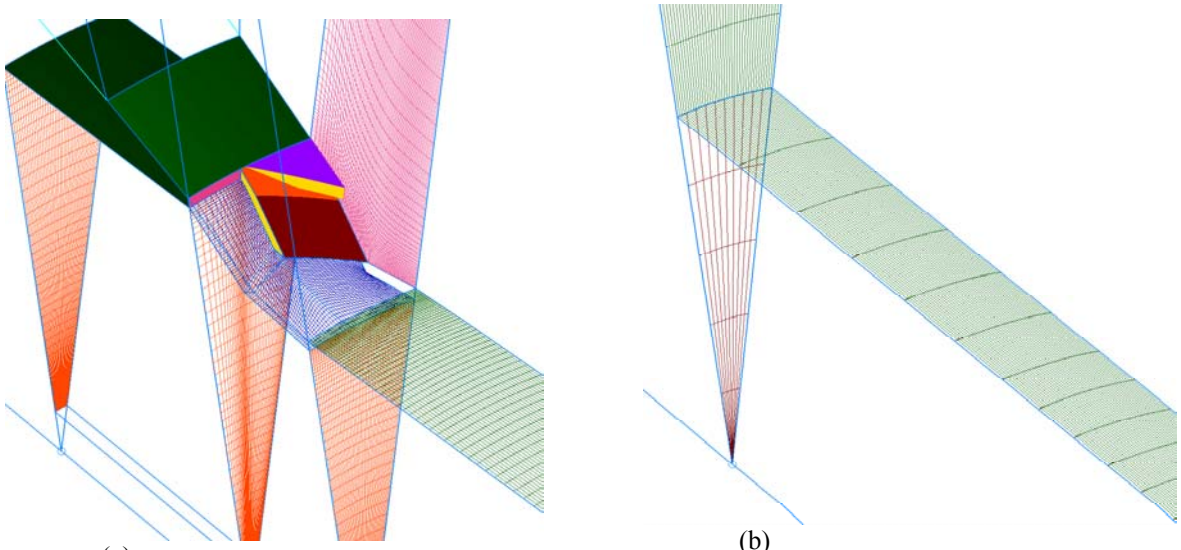

(a) (b)

Figure 2 (a). Grid around the Nozzle Exit and near the Chevrons. Figure 2(a) also Shows all three Chevron Types: (Chevron1: solid purple; Chevron 2: solid orange; Chevron 3: solid red extending from chevron 2) for Comparison. The Nozzle Lip is Pink and the Nozzle Walls and the Cowl are Solid Green in Color.
(b). Non-contiguous Grid Near the Axis Reducing the Azimuthal Grid Points from 41 to 11.

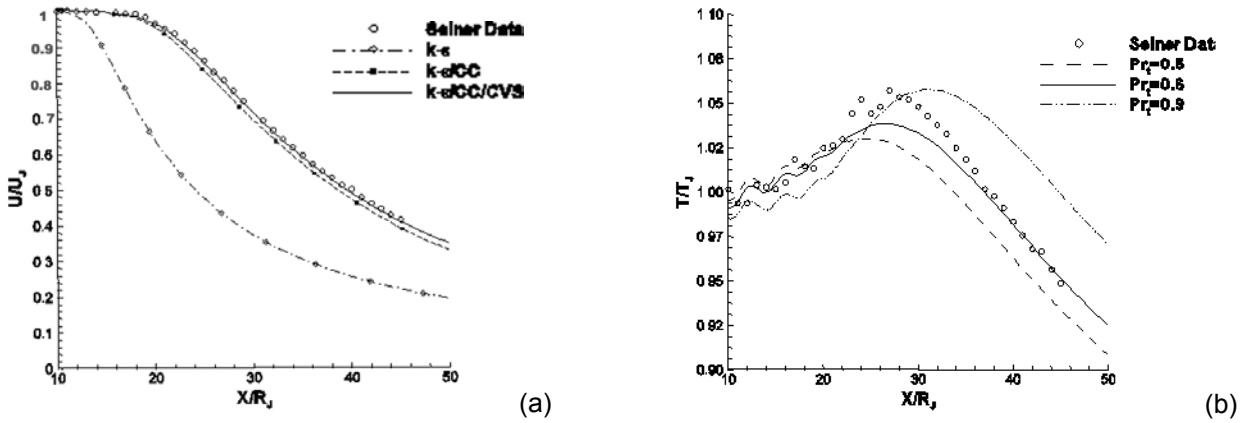

(a) (b)

Figure 3. Turbulence Model Validation for M=2.0 Hot Jet. (a) Mean Streamwise Velocity and (b) Mean Temperature Distribution along the Centerline of the Jet.

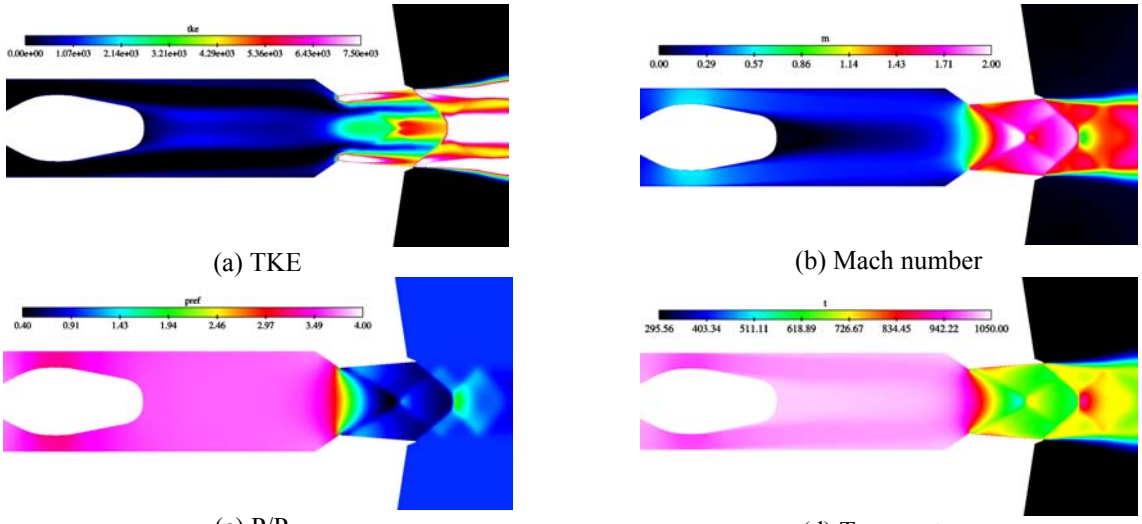

(a) TKE (b) Mach number

(c) P/P_∞ (d) Temperature

Figure 4.1. Contours of TKE, Mach Number, Pressure and Temperature Showing the Wake Effect of the Internal Plug in the Nozzle.

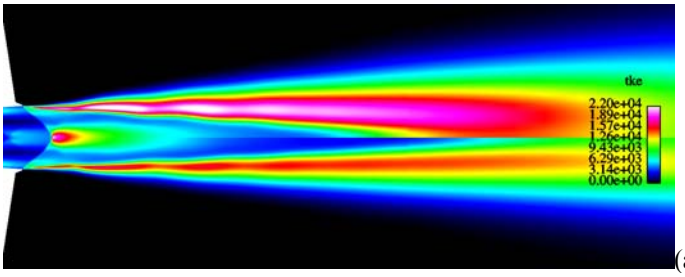

(a)

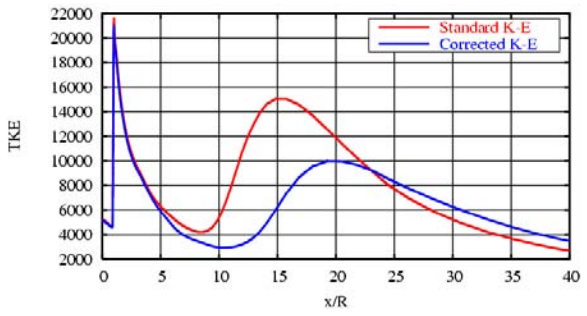

(b)

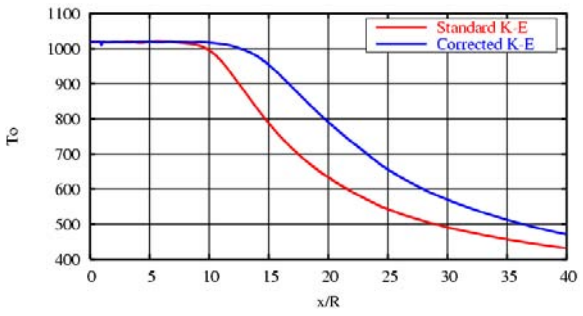

(c)

Figure 4.2. (a) Contours of TKE in xy Plane (Top Half: Standard k-ε Model; Bottom Half: Corrected k-ε Model),
(b) Axial Distribution of TKE, and
(c) Stagnation Temperature Showing the Effect of Turbulence Model for the Baseline Jet.

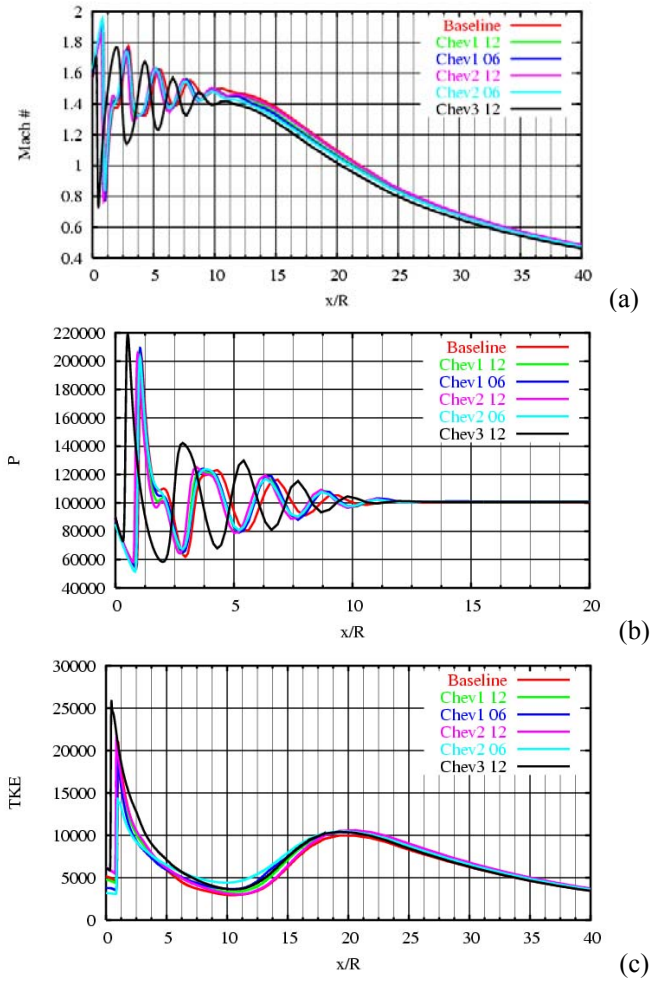

Figure 5. Jet Centerline Distribution of (a) Mach number, (b) Static Pressure and (c) TKE for the Various Nozzle Configurations

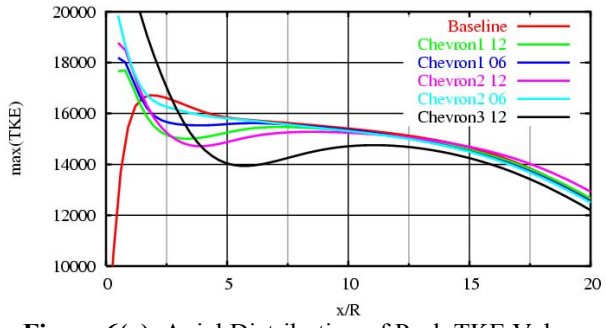

Figure 6(a). Axial Distribution of Peak TKE Values.

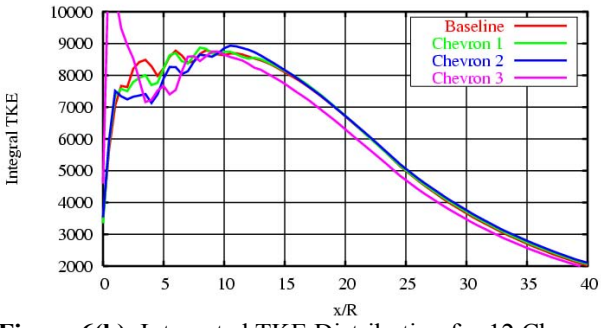

Figure 6(b). Integrated TKE Distribution for 12 Chevron Configurations.

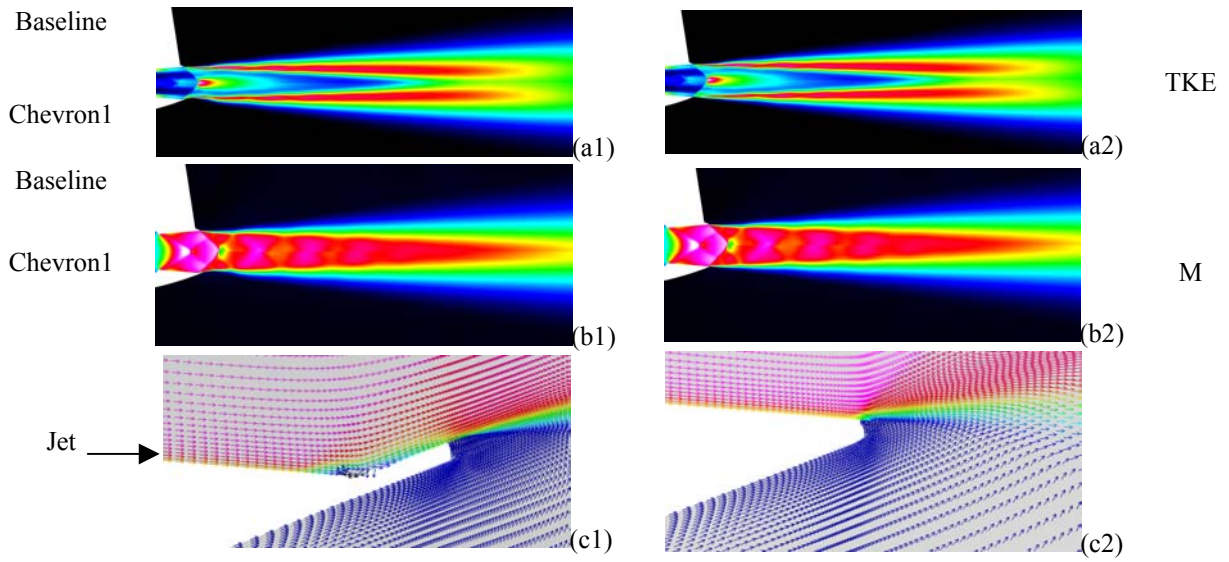

Figure 7. Contours of TKE, Mach number (compared with baseline) and velocity vectors (top to bottom) in the plane of the chevron (left) and in the symmetry plane between 2 chevrons (right) for the Chevron 1 in 12 configuration.

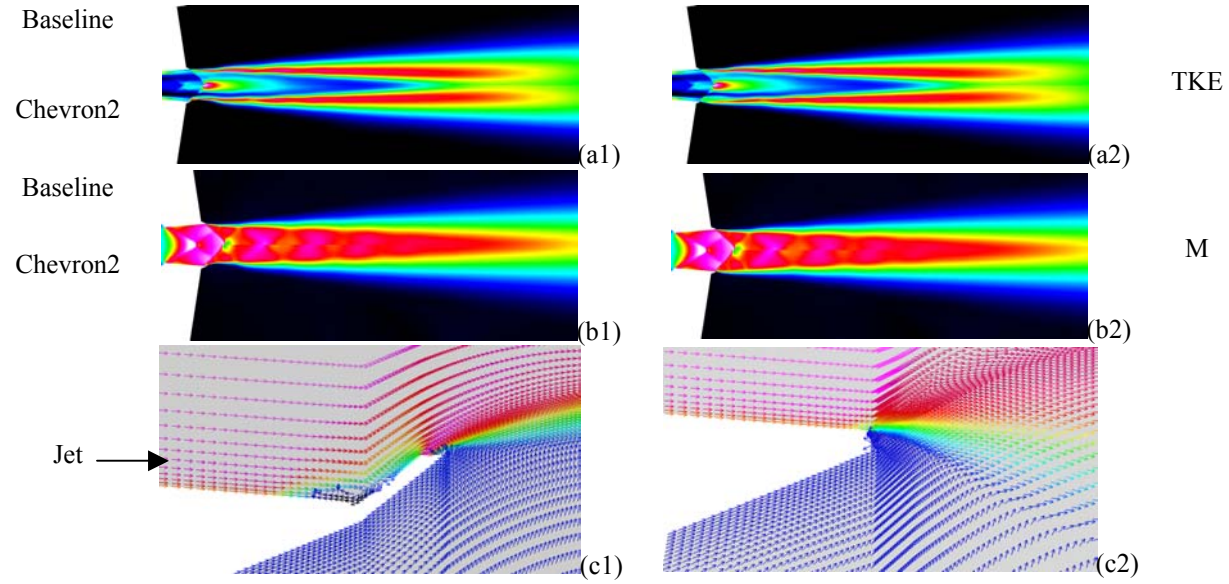

Figure 8. Contours of TKE, Mach number, (compared with baseline) and velocity vectors (top to bottom) in the plane of the chevron (left) and in the symmetry plane between 2 chevrons (right) for the Chevron 2 in 12 configuration.

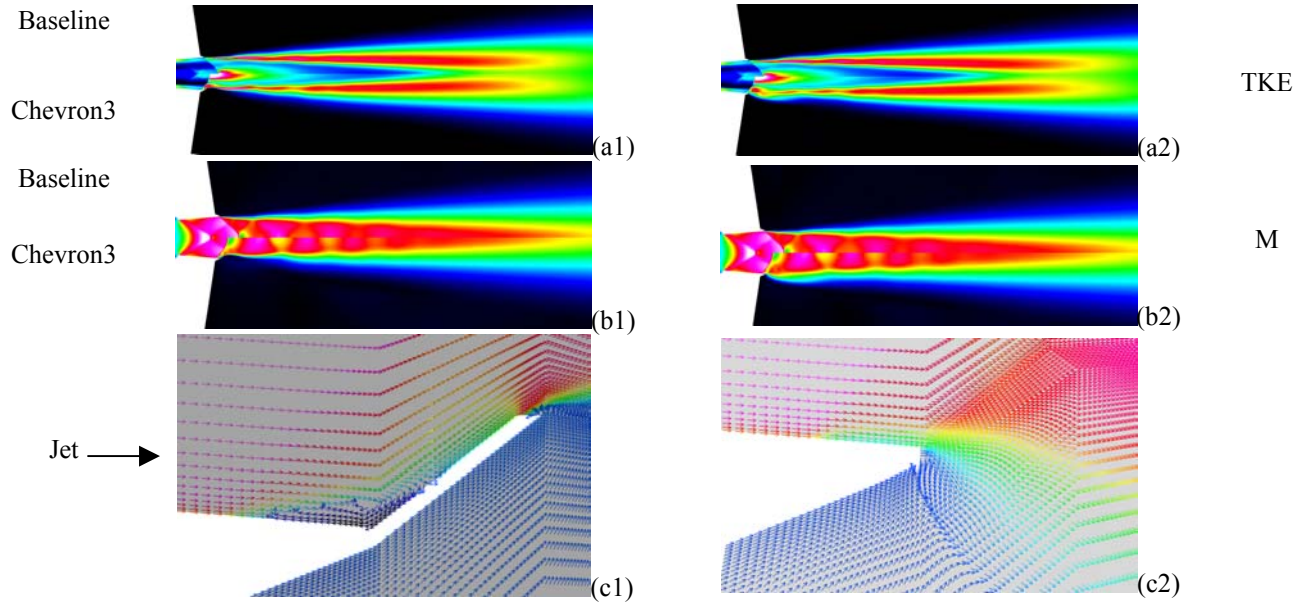

Figure 9. Contours of TKE, Mach number, (compared with baseline) and Velocity Vectors (top to bottom) in the Plane of the Chevron (left) and in the Symmetry Plane Between 2 Chevrons (right) for the Chevron 3 in 12 Configuration.

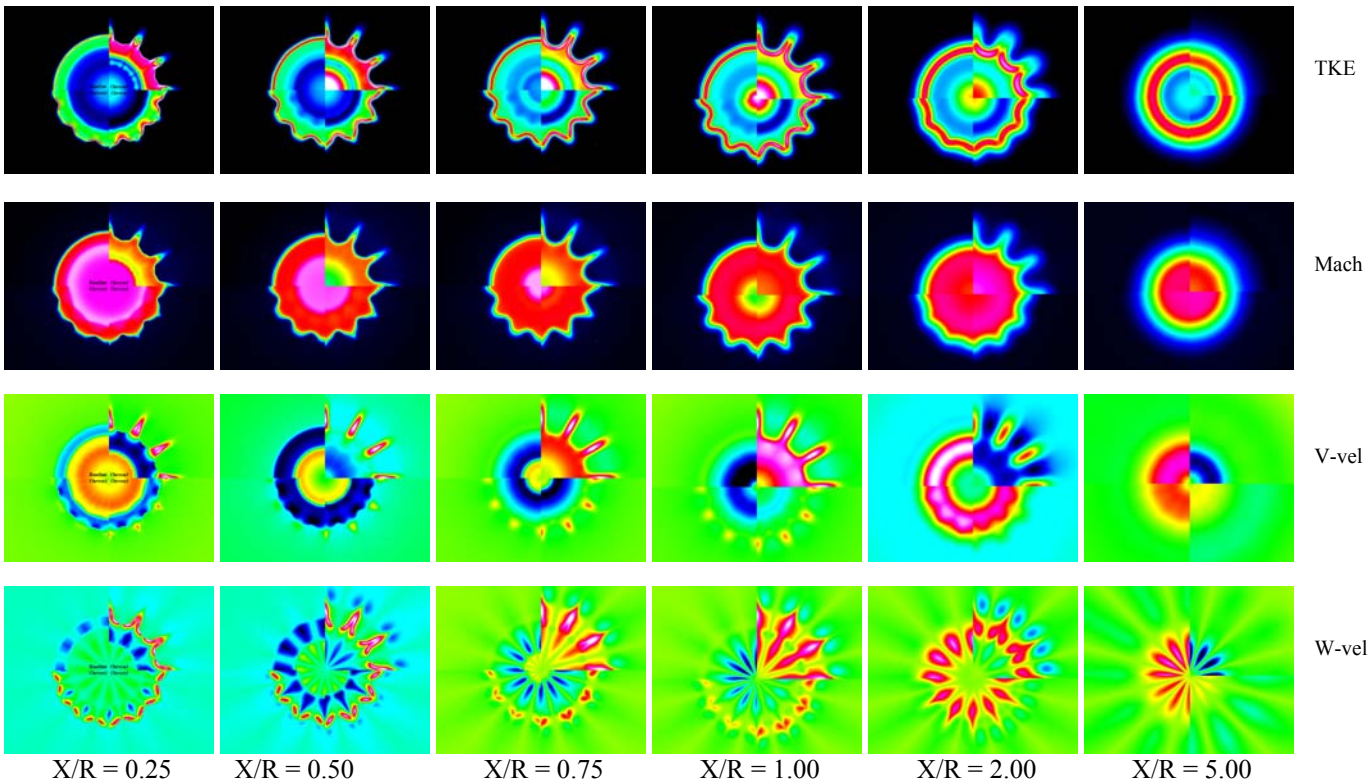

Figure 10. Cross Stream Contours of TKE, Mach Number, v-velocity and w-velocity (top to bottom) for Baseline and the Three Chevrons (in 90 deg. Sectors going anti-clockwise) at x/R = 0.25, 0.50, 0.75,1.00, 2.00, 5.00 (left to right).

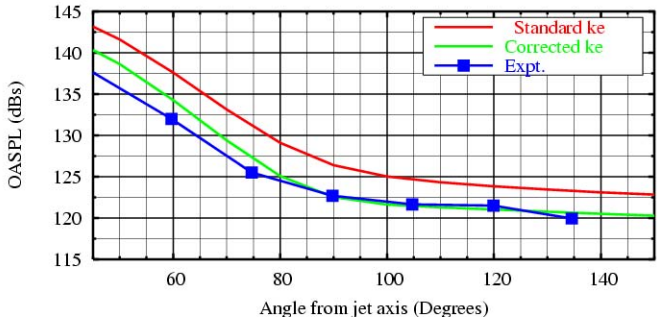

Figure 11. Comparison of OASPL Predictions by Jet3D with that of the Experiment for the Baseline Nozzle.

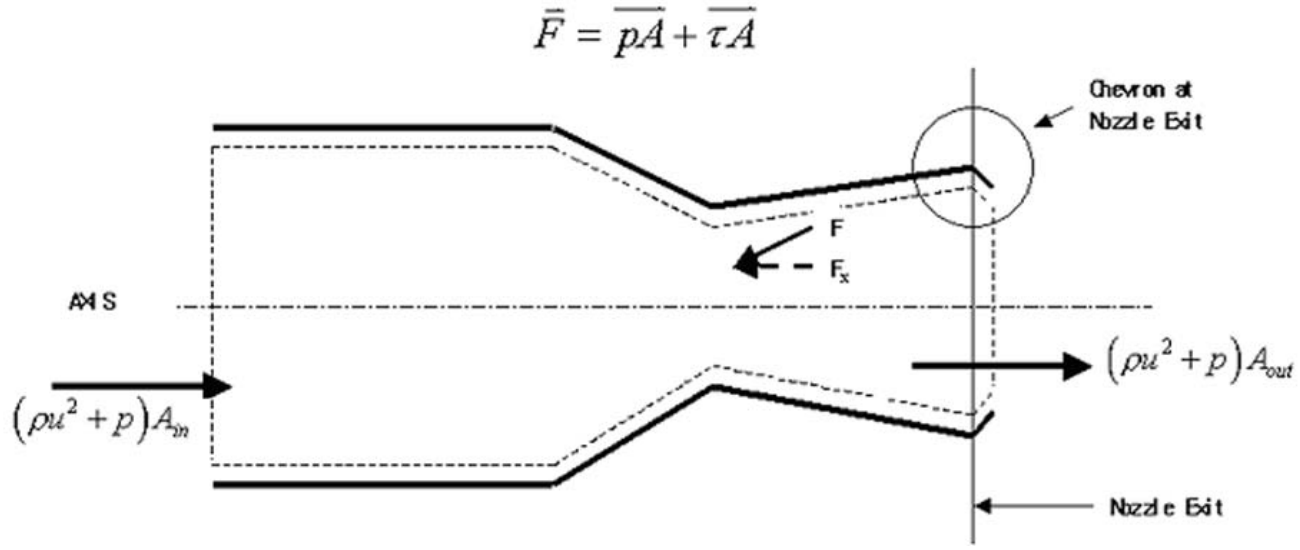

Fig. 12. Schematic of the Control Volume for Thrust Calculation**.**

Table 2. Thrust Prediction for the Nozzle in Various Configurations.

	$(\rho u^2 + p)A_{in}$	F_x (walls)	Net	*N	$(\rho u^2 + p)A_{out}$	% Change
Baseline	58.9372	26.746944	32.190256	24	772.56614	
Chev 1/12	58.9372	27.02037	31.91682	24	766.00391	.85
Chev 1/06	117.66453	53.632793	64.031737	12	768.38084	.54
Chev 2/12	58.9372	27.14748	31.78972	24	762.95328	1.25
Chev 2/06	117.66453	53.772751	63.891779	12	766.70135	.76
Chev 3/12	58.9372	28.579331	30.357869	24	728.58886	5.7
Slotchv 2/06	117.66453	53.6731	63.99143	12	767.89716	.60

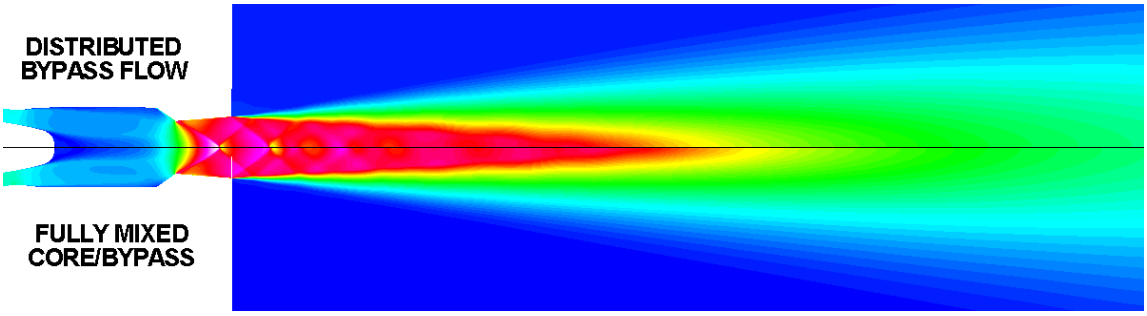

Figure 13. Effect of realistic internal core/bypass mixing on downstream plume: Mach number.

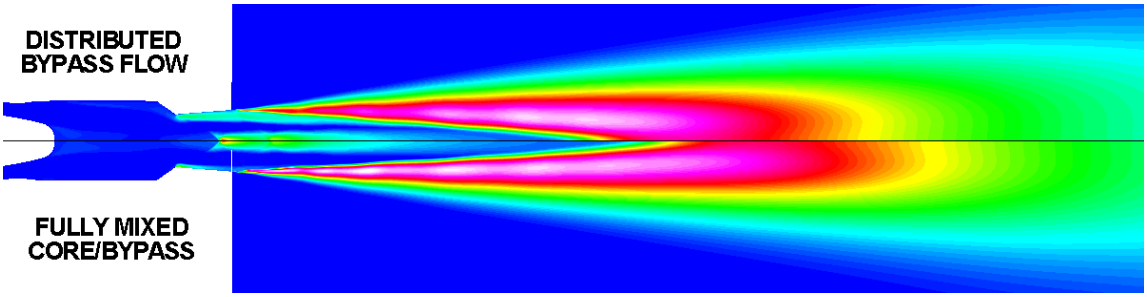

Figure 14. Effect of Realistic Internal Core/Bypass Mixing On Downstream Plume: Turbulent Kinetic Energy.

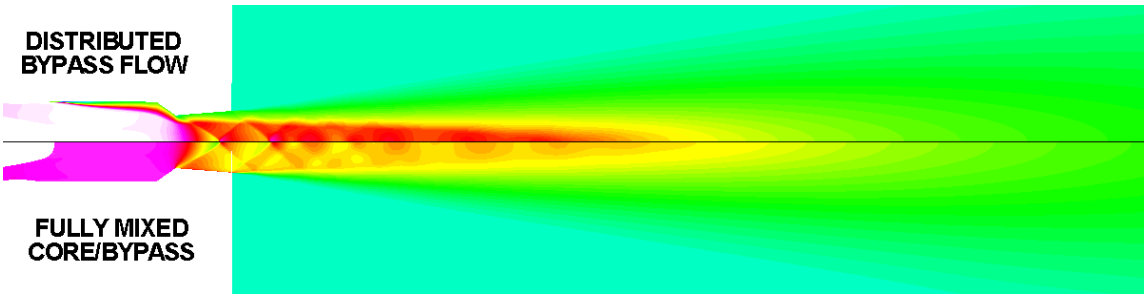

Figure 15. Non-uniform Nozzle Exit Temperature Profile From Upstream Mixing In Realistic F414-400 Augmentor-Nozzle Geometry.

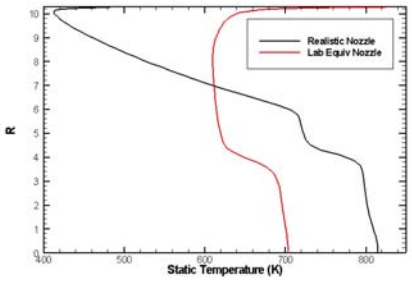

(a) Static temperature.

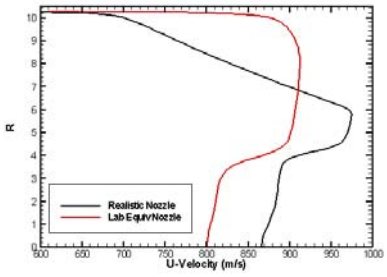

(b) U Velocity.

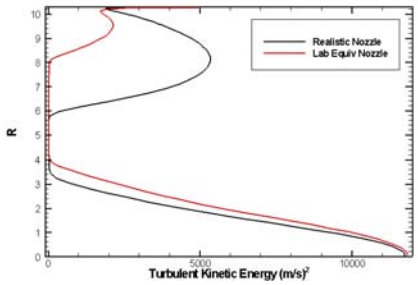

(c) TKE.

Figure 16. Exit Plane Profiles of the Nozzle.

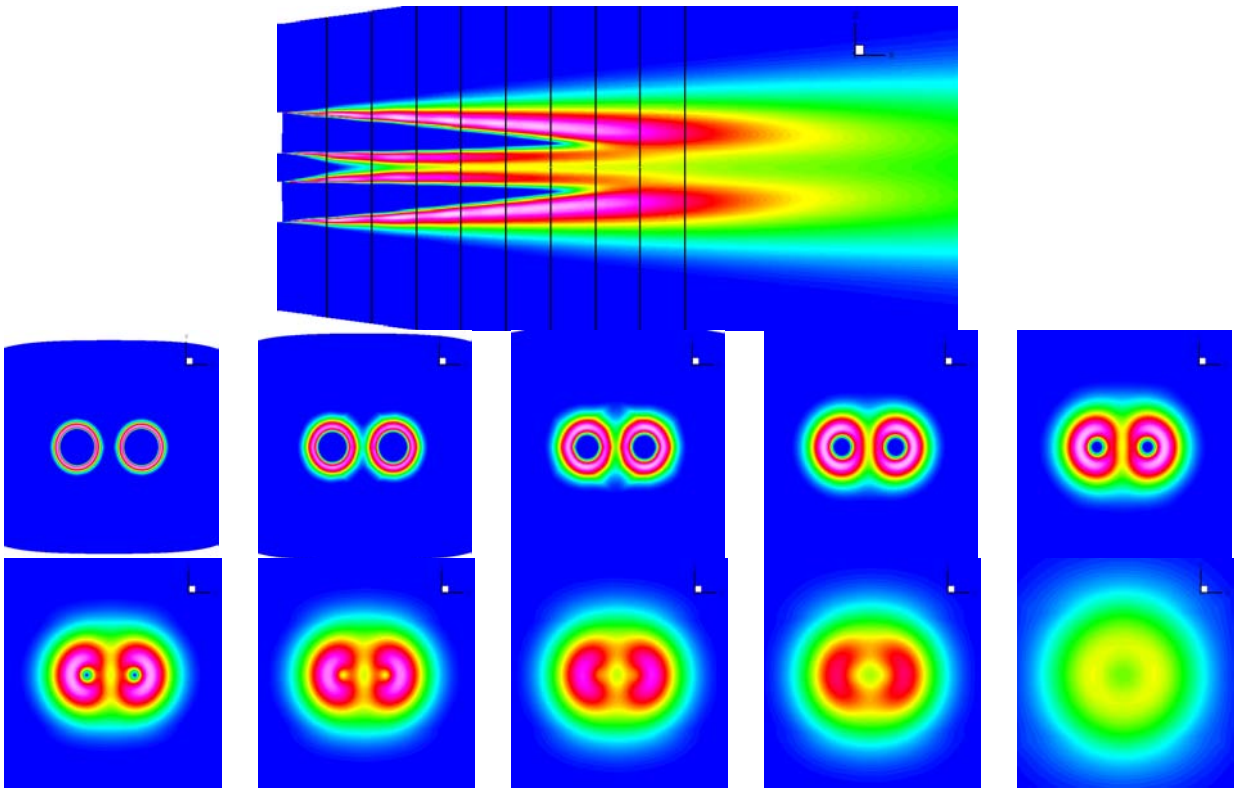

Figure. 17. TKE Contours for Dual Plume Interactions for MRT, Static Surrounding Flow.

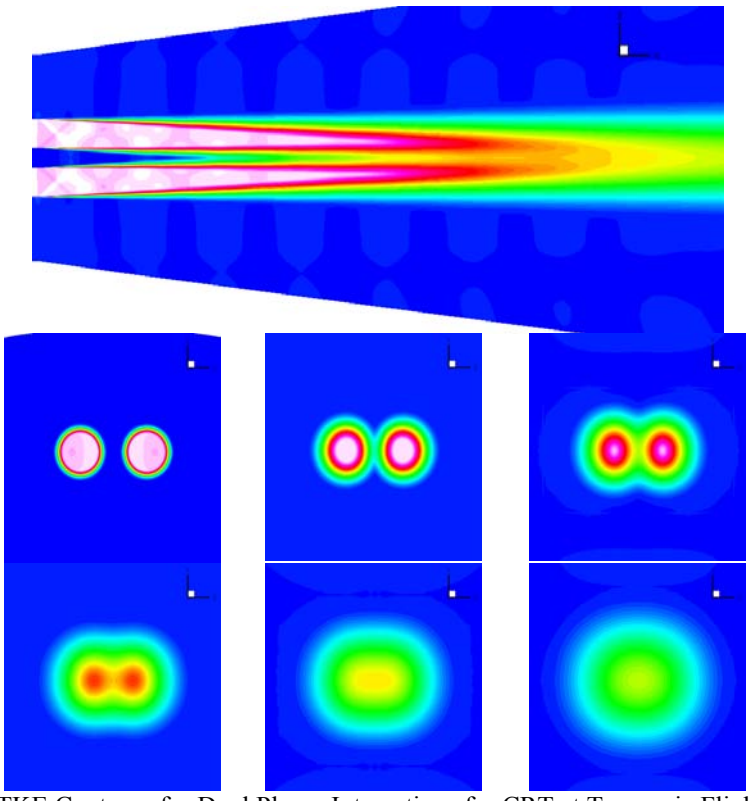

Figure. 18. TKE Contours for Dual Plume Interactions for CRT at Transonic Flight Conditions**.**

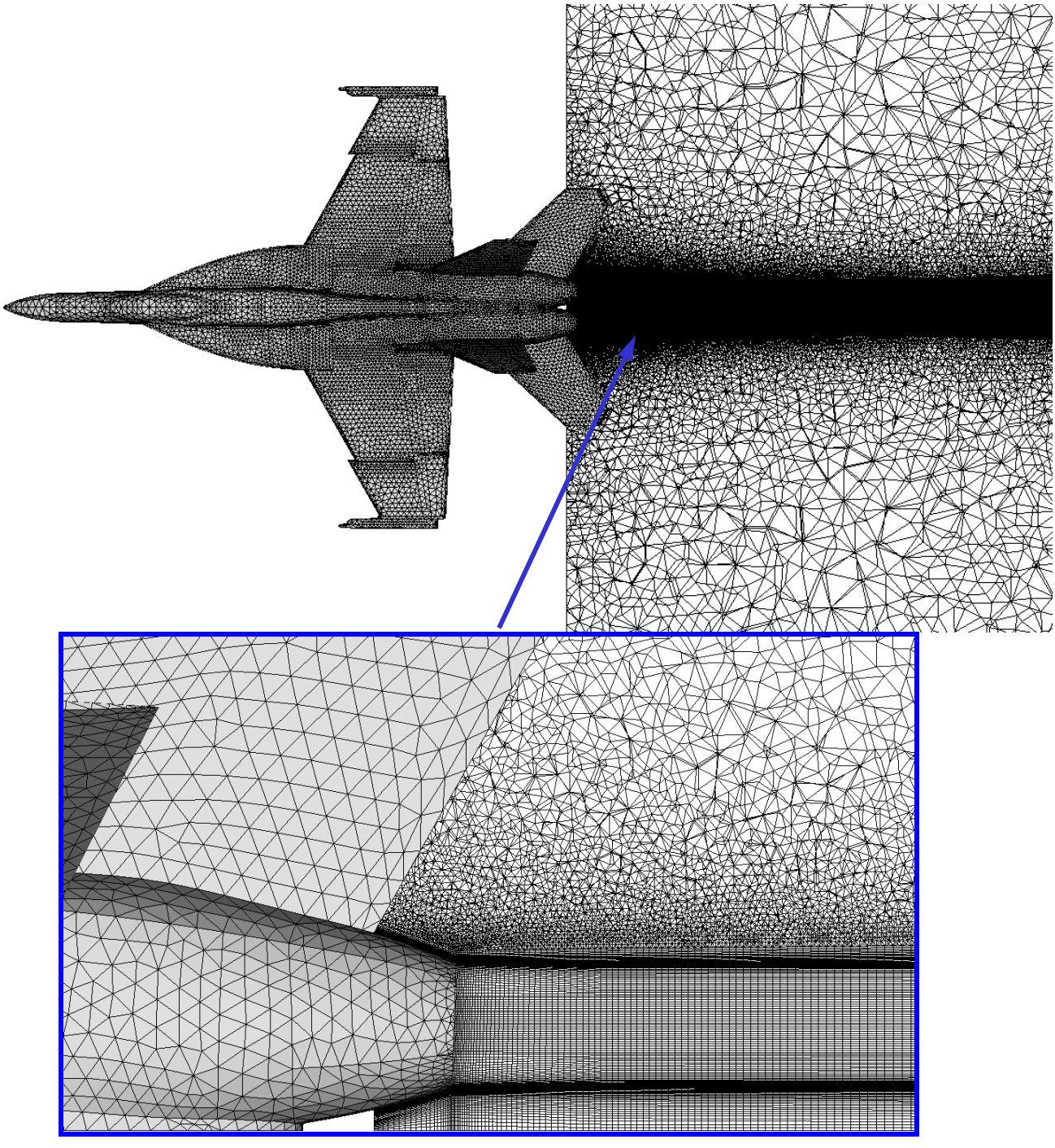

Figure 19. Complete Plume/Aero Calculation**.**

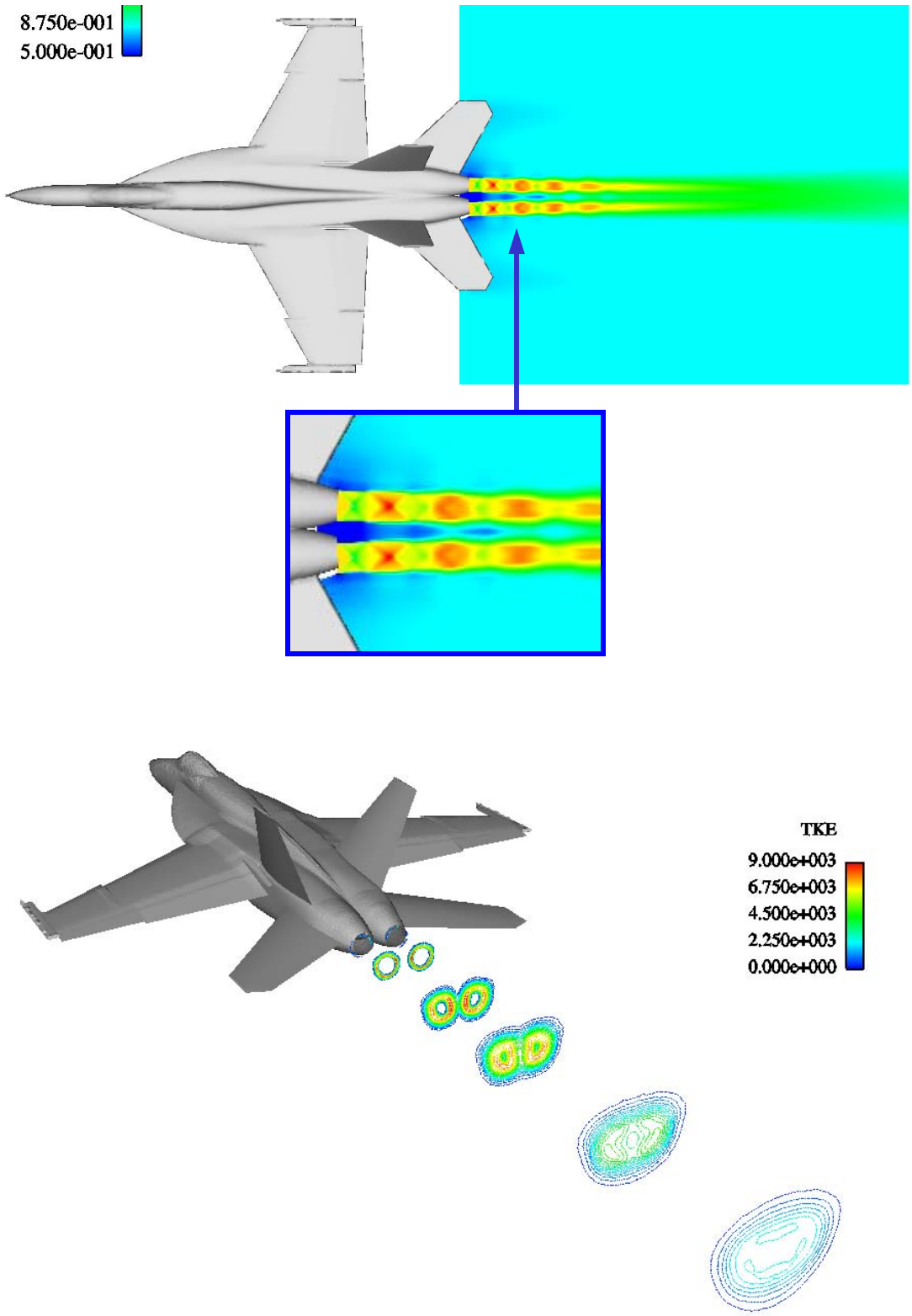

Figure 20. Complete Plume/Aero Calculation; Over-expanded Jet Due to Elevated Pressure at Tail**.**

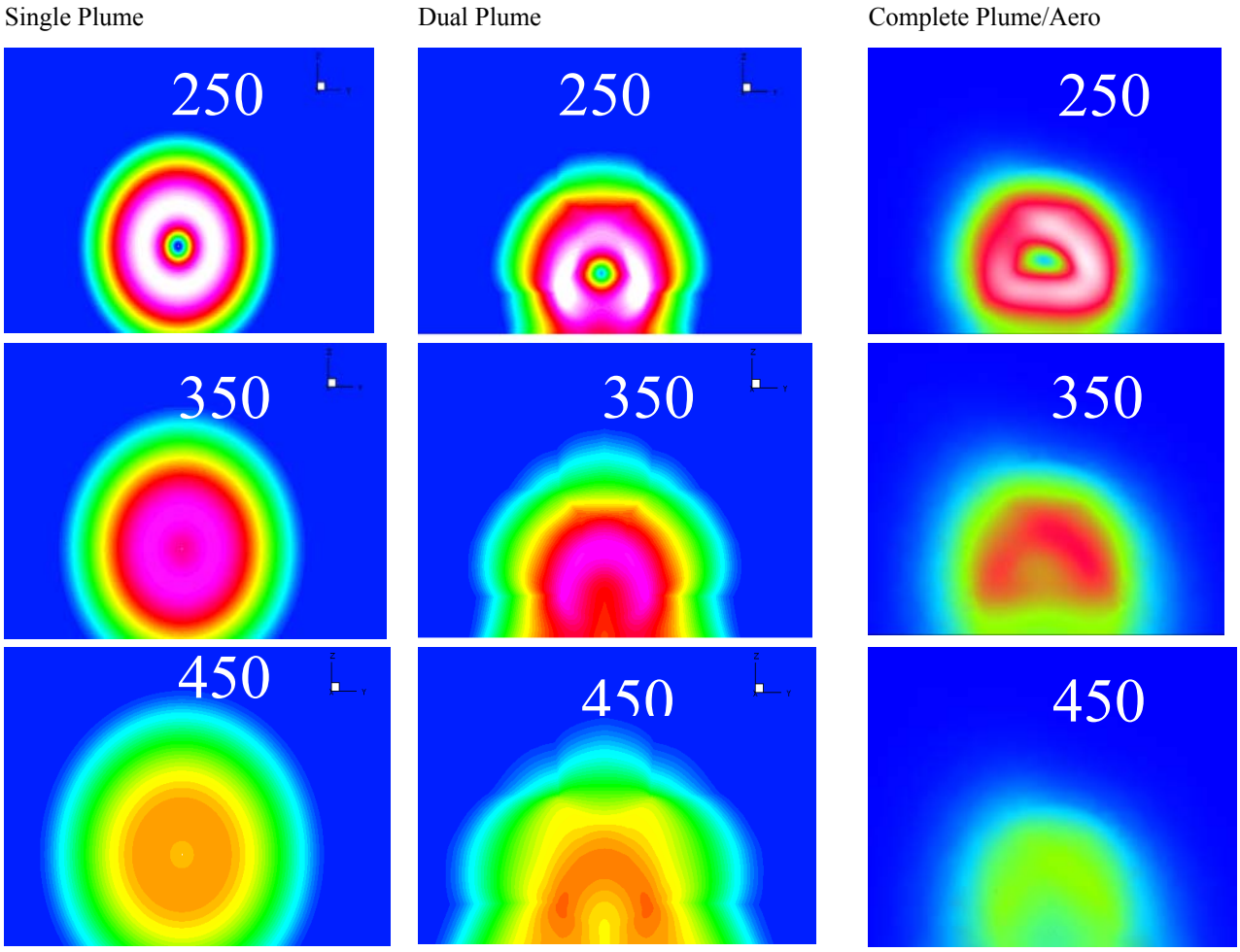

Figure 21. Complete Plume/Aero Calculation; Aerodynamic Effects on Plume.

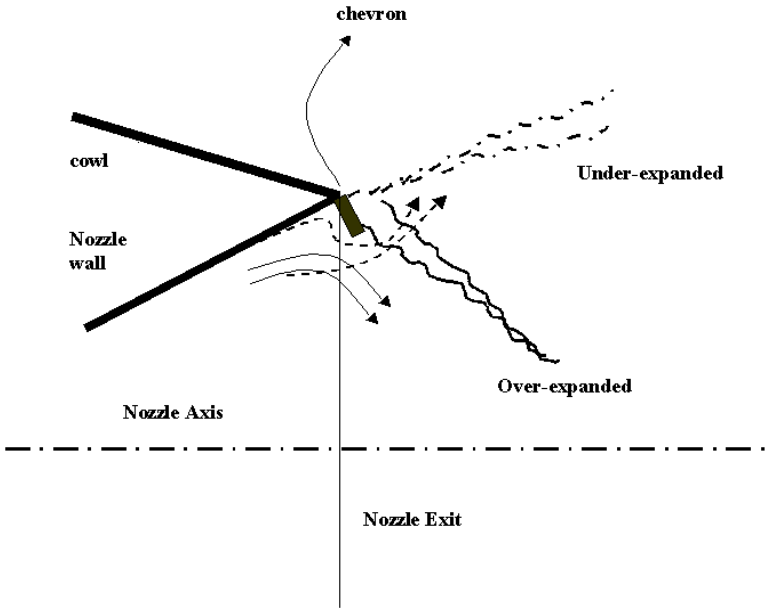

Figure 22. Schematic of Nozzle Exit Flow under Various Conditions.